Dithiolation indolizine exerts viability suppression effects on A549 cells via triggering intrinsic apoptotic pathways and inducing G2/M phase arrest

Guanting Li[a,b], Xianwei Wu[a,b], Peng Sun[c], Zhiyang Zhang[a,b], Enxian Shao[a,b], Jianping Mao[a], Hua Cao[d,**], Hongliang Huang[a,e,*]

[a] School of Biosciences & Biopharmaceutics and Guangdong Province Key Laboratory for Biotechnology Drug Candidates, Guangdong Pharmaceutical University, Guangzhou 510006, China
[b] School of Pharmacy, Guangdong Pharmaceutical University, Guangzhou 510006, China
[c] Sun Yat-sen University Cancer Center, State Key Laboratory of Oncology in South China, Collaborative Innovation Center for Cancer Medicine, 651 Dongfeng Road East, Guangzhou, Guangdong Province, 510060, China
[d] School of Chemistry and Chemical Engineering, Guangdong Pharmaceutical University, Zhongshan, China
[e] Key Laboratory of New Drug Discovery and Evaluation, Guangdong Pharmaceutical University, Guangzhou 510006, China

ARTICLEINFO

Keywords:
A549 cells
Apoptosis
G2/M arrest
Endoplasmic reticulum stress (ERS)
Mitochondrial pathway

ABSTRACT

Indolizine derivatives have been reported for the treatment of numerous diseases. However, few studies were carried out for non-small cell lung cancer (NSCLC). We synthesized series of indolizine compounds. The results of MTT assay showed compound 8 (C8) markedly inhibited the proliferation of A549 cells, however, C8 (15, 30 μg/ mL) had little cytotoxicity in other cell lines (SH-SY5Y, HepG2, and BEAS-2B cells), Hoechst staining and JC-1 staining showed that C8 induced changes in the nucleus morphology, increased the loss in mitochondrial membrane potential in A549 cells. The results of flow cytometry manifested that cell cycle of the cells was arrested in the G2 / M phase by C8, ROS levels and the proportion of apoptosis of cells increased. We performed western blotting analysis to detect the expression levels of apoptosis and cycle-related proteins. These results validated that the apoptosis of cells was triggered by endoplasmic reticulum stress (ERS) and the PI3K/Akt- mediated mitochondrial pathway collaboratively. Besides, the utilization of PI3K/Akt inhibitors and p53 inhibitors further proves the above argument and C8-induced cycle arrest of A549 cells is majorly regulated by p53. C8 induced the accumulation of ROS contents involved in mitochondrial damage. The proliferation of A549 cells was inhibited after treatment with the compound, which induced apoptosis and cycle arrest of cells. It is suggested that C8(dithiolation indolizine) is a potential candidate compound against non-small cell lung cancer.

1. Introduction

Lung cancer has contributed to the one of main causes of cancer- related deaths in the world [1]. Non-small cell lung cancer (NSCLC) is a relatively common type of lung cancer, and it has been proved to spread at an early stage of cancer and is sensitive to chemotherapy simultaneously [2,3]. Surgery is usually an option. But multiple surgeries are likely to increase the risk of infection for cancer patients. It is well known that chemotherapy requires simple conditions, less expensive equipment, which reduces the risk of infection and costs. Chemotherapy is important for therapy NSCLC [4], and it is significantly worthy to look for anticancer candidates for the disease.

Indolizine, a hexa-5 heterocyclic ring containing a ring nitrogen. The aromatic indolizine ring is relatively rare in nature, but it is common in its fully hydrogenated product, which is found in many alkaloids [5,6]. It has been widely concerned due to its biological activities such as anti-inflammatory [7], antibacterial [8], and anti-oxidation [9]. Indolizine was reported for the treatment of diabetes [10] and schizophrenia [11]. We have reported a novel synthetic method, which is for the first time to develop an efficient transition-metal(1)-free regioselective
C–H/SH– cross-coupling of indolizines with thiols for the first time providing a workable route to indolizine thioethers.

In this study, the newly synthesized compounds were screened against the non-small cell lung cancer cells (A549 cells). Based on screening out the active compound, we further explored the sensitivity of the compound to cancer cell lines of the different tissue origin (the SH- SY5Y neuroblastoma cells, liver cancer HepG2 cells) and non-cancer cell line of the same tissue origin (normal human bronchial epithelial BEAS- 2B cells). Finally, the effects and the mechanism will be explored.

2. Methods

2.1. Reagents and materials

Dimethyl sulfoxide cell culture reagent (DMSO, MP Biomedicals, France), 3-(4, 5-dimethyl-2-tetrazolyl)-2, 5-diphenyltetrazolium bromide (MTT, Waltham, MA, USA), N-acetyl -L-cysteine (NAC, Macklin Biochemical, China), Pifithrin-α (PF, S2929, Selleck chemicals) and LY294002 (LY, S1105, Selleck chemicals). Hoechst 33342(#C1026), Cell Cycle and Apoptosis Analysis Kit(#C1052), Mitochondrial membrane potential assay kit with JC-1(#C2006), Annexin V-FITC Apoptosis Detection Kit(#C1062 L), Reactive Oxygen Species Assay Kit(#C0033) were bought from the Beyotime Biotechnology Inc (China).

2.2. Cells and compound samples preparation

The human NSCLC cells (A549 cells) were cultured with Roswell Park Memorial Institute 1640 Medium

* Corresponding author at: School of Biosciences & Biopharmaceutics and Guangdong Province Key Laboratory for Biotechnology Drug Candidates, Guangdong Pharmaceutical University, 510006, Guangzhou, China.
** Corresponding author.
E-mail addresses: caohua@gdpu.edu.cn (H. Cao), huanghl@gdpu.edu.cn (H. Huang).

https://doi.org/10.1016/j.biopha.2020.110961
Received 14 May 2020; Received in revised form 30 October 2020; Accepted 1 November 2020
Available online 12 November 2020
0753-3322/© 2020 The Authors. Published by Elsevier Masson SAS. This is an open access article under the CC BY-NC-ND license (http://creativecommons.org/licenses/by-nc-nd/4.0/).

(RPMI 1640 Medium, Gibco, USA). The normal lung epithelial cells (BEAS-2B cells), the human SH- SY5Y neuroblastoma cells and the human liver cancer HepG-2 cells were cultured in Dulbecco's Modified Eagle's Medium (DMEM). All cell lines were supplemented with 10 % FBS (Waltham, MA, USA), 1% penicillin -streptomycin (100 μg/mL; Hyclone, USA) with CO_2 (5%), at 37 °C in a humidified atmosphere incubator (Thermo Scientific, USA).

The series of compounds were dissolved in DMSO to formulate into a 10 mg/mL solution.

2.3. Chemistry

A solution of 2-picoline (0.93 g, 10 mmol, 1.0 equiv.) and 2-bromoacetophenone (1.99 g, 10 mmol, 1.0 equiv) in acetone (50 mL) was heated at 60 ℃ for 5 h. The resulting precipitate was isolated via filtration and redissolved in 20 mL of hot water (60 ℃). Then, K_2CO_3 (1.38 g, 10 mmol, 1.0 equiv) was added, and the mixture was heated at 60 ℃for 5 h. After filtration and drying in vacuum the compound 1a was obtained as a white solid in 50 % overall yield (965 mg, 5 mmol). With an optimized catalytic system in hand, we next explored the scope and generality of this cross-coupling reaction by examining a variety of thiols in the presence of 5 mol % of KI and TBHP in a test tube at 60 °C for 4 h [12].

2.4. Characterization of compounds

2-Phenyl-1,3-bis(propylthio)indolizine (C1, 93 %)

Yellow oil. 63.4 mg. IR (KBr): 3051, 2960, 1564, 752, 701 cm^{-1};^{1}H NMR (400 MHz, CDCl3) *δ* 8.52 (d, *J* =7.2 Hz, 1 H), 7.76 (d, *J* =8.8 Hz, 1 H), 7.58 (d, *J* =8.0 Hz, 2 H), 7.45 (t, *J* =7.6 Hz,2 H), 7.36 (t, *J* =7.2 Hz, 1
H), 6.96− 6.89 (m, 1 H), 6.70 (t, *J* =7.2 Hz, 1 H), 2.43 (t, *J* =7.2 Hz, 2
H),2.36(t, *J* =7.2 Hz, 2 H), 1.28 (dt, *J* = 13.2, 7.2 Hz, 4 H), 0.79− 0.74 (m, 3 H), 0.76− 0.72 (m, 3 H). ^{13}C NMR (100 MHz, CDCl3) *δ* 139.9, 137.8, 134.5, 131.0, 131.0, 127.6, 127.6, 126.9, 124.0, 120.0, 117.9, 111.6, 111.2, 101.1, 39.2, 37.6, 22.6, 22.6, 13.0, 12.9. ESI-MS *m/z* (%) 341 (100) $[M+H]^+$; Anal. Calcd for C20H23NS2 C, 70.34; H, 6.79; N, 4.10; Found: C, 70.35; H, 6.78; N, 4.10.

1,3-Bis(ethylthio)-2-phenylindolizine (C2, 86 %)

Yellow oil. 53.8 mg. IR (KBr): 3031, 2965, 1554, 755, 706 cm^{-1};^{1}H NMR (400 MHz, $CDCl_3$) δ8.53 (d, J =7.2 Hz, 1 H), 7.75 (d, J =8.8 Hz, 1 H), 7.57 (d, J =8.0 Hz, 2 H), 7.45 (t, J =7.6 Hz, 2 H), 7.37 (t, J =7.2 Hz, 1
H), 6.97− 6.91 (m, 1 H), 6.70 (t, J =6.8 Hz, 1 H), 2.49 (q, J =7.2 Hz, 2
H), 2.41 (q, J =7.2 Hz, 2 H), 0.98− 0.95 (m, 3 H), 0.95− 0.92 (m, 3 H). ^{13}C NMR (100 MHz, $CDCl_3$) δ 140.1, 138.1, 134.5, 131.0, 127.6, 127.0, 124.1, 120.2, 117.9, 111.6, 111.0, 100.8, 31.0, 29.7, 14.8, 14.6.ESI-MS m/z (%) 313 (100) $[M+H]^+$; Anal. Calcd for C18H19NS2 C, 68.97; H, 6.11; N, 4.47; Found: C, 68.99; H, 6.11; N, 4.46.

1,3-Bis(butylthio)-2-phenylindolizine (C3, 91 %)

Yellow oil. 67.2 mg. IR (KBr): 3043, 2953, 1562, 764, 712 cm^{-1};^{1}H NMR (400 MHz, $CDCl_3$) *δ*8.52 (d, *J* =7.2 Hz, 1 H), 7.73 (d, *J* =8.8 Hz, 1 H), 7.59 (d, *J* =7.6 Hz, 2 H), 7.46 (t, *J* =7.6 Hz, 2 H),7.36 (t, *J* =7.2 Hz, 1
H), 6.93 (d, *J* =9.6 Hz, 1 H), 6.70 (t, *J* =6.4 Hz, 1 H), 2.46 (t, *J* =7.2 Hz, 2
H), 2.38 (t, *J* =6.8 Hz, 2 H), 1.28− 1.12 (m, 8 H), 0.74− 0.66 (m, 6 H). ^{13}C NMR (100 MHz, $CDCl_3$) *δ*139.9, 137.8, 134.5, 131.0, 127.6, 127.0, 124.1, 120.1, 117.9, 111.6, 111.3, 101.1, 36.8, 35.3, 31.4, 31.3, 21.5, 21.4, 13.6, 13.5. ESI-MS *m/z* (%) 369 (100) $[M+H]^+$; Anal. Calcd for C22H27NS2 C, 71.50; H, 7.36; N, 3.79; Found: C, 71.52; H, 7.35; N, 3.78.

1,3-Bis(dodecylthio)-2-phenylindolizine (C4, 89 %)

Yellow oil. 105.7 mg. IR (KBr): 3048, 2949, 1566, 752, 708 cm^{-1}; ^{1}H NMR (400 MHz, $CDCl_3$) *δ*8.52 (d, *J* =6.8 Hz, 1 H), 7.73 (d, *J* =8.8 Hz, 1 H), 7.58 (d, *J* =7.6 Hz, 2 H), 7.44 (t, *J* =7.6 Hz, 2 H), 7.35 (t, *J* =7.2 Hz, 1 H), 6.92 (dd, *J* = 8.8, 6.4 Hz, 1 H), 6.69 (t, *J* =6.8 Hz, 1 H), 2.43 (t, *J* =7.2 Hz, 2 H), 2.37 (t, J =7.2 Hz, 2 H), 1.30− 1.05 (m, 40 H), 0.87 (t, J =6.7 Hz, 6 H). ^{13}C NMR (100 MHz,CDCl3) *δ* 139.9, 137.8, 134.5, 131.1, 127.6, 127.0, 124.1, 120.0, 118.0, 111.6, 111.2, 101.1, 37.2, 35.6, 31.9, 31.9, 29.6, 29.6, 29.6, 29.6, 29.5, 29.5, 29.4, 29.3, 29.3, 29.3, 29.3, 29.2, 29.1, 29.1, 28.4, 28.4, 22.7, 22.7, 14.1, 14.1. ESI-MS *m/z* (%) 594 (100) $[M+H]^+$; Anal. Calcd for C38H59NS2 C, 76.84; H, 10.01; N, 2.36; Found: C, 76.82; H, 10.01; N, 2.35.

1,3-Bis(isopropylthio)-2-phenylindolizine (C5, 80 %)

Yellow oil. 54.6 mg. IR (KBr): 3047, 2950, 1575, 780, 722 cm^{-1};^{1}H NMR (400 MHz, CDCl3) *δ*8.59 (d, *J* =7.2 Hz, 1 H), 7.75 (d, *J* =8.8 Hz, 1 H), 7.58 (d, *J* =8.0 Hz, 2 H), 7.44 (t, *J* =7.6 Hz,2 H), 7.35 (t, *J* =7.2 Hz, 1
H), 6.98− 6.86 (m, 1 H), 6.70 (t, *J* =7.2 Hz, 1 H), 2.96 (p, *J* =6.8 Hz, 1 H), 2.75(p, *J* =6.8 Hz, 1 H), 0.98 (d, *J* =6.8 Hz, 12 H). ^{13}C NMR (100 MHz, CDCl3) *δ* 140.8, 138.6, 134.7, 131.3, 127.4, 126.8, 124.3, 120.3, 118.1, 111.5, 111.3, 100.5, 40.2, 40.1, 23.0, 23.0. ESI-MS *m/z* (%) 341 (100) $[M+H]^+$; Anal. Calcd for C20H23NS2 C, 70.34; H, 6.79; N, 4.10; Found:
C, 70.36; H, 6.79; N, 4.11.

1,3-Bis(sec-butylthio)-2-phenylindolizine (C6, 59 %)

Yellow oil. 43.5 mg. IR (KBr): 3035, 2946, 1561, 762, 708 cm^{-1};^{1}H NMR (400 MHz, CDCl3) *δ* 8.57 (d, *J* =7.2 Hz, 1 H), 7.73 (d, *J* =8.8 Hz, 1 H), 7.57 (d, *J* =8.0 Hz, 2 H), 7.42 (t, *J* =7.6 Hz,2 H), 7.34 (t, *J* =7.2 Hz, 1
H), 6.95− 6.91 (m, 1 H), 6.70 (t, *J* =7.2 Hz, 1 H), 2.71 (q, *J* =6.8 Hz, 1
H),2.51(q, *J* =6.8 Hz, 1 H), 1.36− 1.30 (m, 2 H), 1.26− 1.19 (m, 2 H), 0.93 (d, *J* =6.8 Hz, 6 H), 0.72 (t, *J*=7.2 Hz, 6 H). ^{13}C NMR (100 MHz, CDCl3) *δ* 141.0, 138.6, 134.7, 131.4, 127.4, 126.8, 124.3, 120.1, 118.1, 111.4, 111.1, 100.4, 47.1, 46.9, 29.3, 29.3, 20.5, 20.3, 11.3, 11.1. ESI- MS *m/z* (%) 369 (100) $[M+H]^+$; Anal. Calcd for C22H27NS2 C, 71.50; H, 7.36; N, 3.79; Found: C, 71.51; H, 7.37; N, 3.79.

1,3-Bis(isopentylthio)-2-phenylindolizine (C7, 77 %)

Yellow oil. 61.1 mg. IR (KBr): 3051, 2960, 1564, 752, 701 cm^{-1};^{1}H NMR (400 MHz, CDCl3) *δ*8.53 (d, *J* =7.2 Hz, 1 H), 7.73 (d, *J* =9.6 Hz, 1 H), 7.59 (d, *J* =7.2 Hz, 2 H), 7.45 (t, *J* =7.6 Hz, 2 H), 7.37 (t, *J* =8.0 Hz, 1
H), 6.96− 6.90 (m, 1 H), 6.71 (t, *J* =6.0 Hz, 1 H), 2.47 (t, *J* =7.6 Hz, 2 H),
2.39(t, *J* =6.8 Hz, 2 H), 1.52− 1.39 (m, 2 H), 1.17 (p, *J* =8.0 Hz, 4 H), 0.70 (d, *J* =7.2 Hz, 12 H). ^{13}C NMR

(100 MHz, CDCl3) δ 139.7, 137.7, 134.4, 131.0, 127.6, 127.0, 124.1, 120.0, 117.9, 111.6, 111.3, 101.2, 38.3, 38.1, 35.1, 33.6, 26.8, 26.8, 22.2, 22.2, 22.0, 22.0. ESI-MS *m/z* (%) 397 (100) $[M+H]^+$; Anal. Calcd for C24H31NS2 C, 72.49; H, 7.86; N, 3.52; Found: C, 72.50; H, 7.87; N, 3.52.

1,3-Bis(benzylthio)-2-phenylindolizine(C8, 83 %)

Yellow oil. 72.5 mg. IR (KBr): 3031, 2932, 1576, 725, 689 cm^{-1};^{1}H NMR (400 MHz, CDCl3) δ8.11 (d, *J* =7.2 Hz, 1 H), 7.38 (d, *J* =7.6 Hz, 3

H), 7.31− 7.26 (m, 3 H), 7.10− 7.02 (m, 6 H), 6.86 (d, *J*=7.6 Hz, 2 H),

6.80 (d, *J* =8.0 Hz, 2 H), 6.73− 6.69 (m, 1 H), 6.44 (t, *J* =6.8 Hz, 1 H),

3.60 (s, 2 H), 3.52 (s, 2 H). ^{13}C NMR (100 MHz, CDCl3) δ 140.4, 138.3, 138.1, 137.4, 133.9, 130.6, 128.6, 128.5, 128.1, 127.9, 127.4, 126.9, 126.8, 126.4, 123.6, 120.2, 117.3, 111.2, 110.2, 100.0, 41.4, 40.4.ESI- MS *m/z* (%) 437 (100) $[M+H]^+$; Anal. Calcd for C28H23NS2 C, 76.85; H, 5.30; N, 3.20; Found: C, 76.83; H, 5.31; N, 3.21.

1,3-Bis(cyclohexylthio)-2-phenylindolizine (C9, 78 %)

Yellow oil. 69.4 mg. IR (KBr): 3046, 2926, 1554, 732, 712 cm^{-1};^{1}H NMR (400 MHz, CDCl3) δ8.58 (d, *J* =7.2 Hz, 1 H), 7.75 (d, *J* =8.8 Hz, 1 H), 7.55 (d, *J* =8.0 Hz, 2 H), 7.43 (t, *J* =7.6 Hz, 2 H), 7.34 (t, *J* =7.2 Hz, 1

H), 6.94− 6.86 (m, 1 H), 6.70− 6.63 (m, 1 H), 2.65 (s, 1 H), 2.47 (s, 1 H), 1.65− 1.51 (m, 8 H), 1.41 (s, 2 H), 1.08 (m, 10 H). ^{13}C NMR (100 MHz, CDCl3) δ 141.0, 138.5, 134.8, 131.4, 127.4, 126.7, 124.3, 120.1, 118.1, 111.4, 110.7, 100.1, 48.6, 48.3, 33.2, 33.2, 33.2,33.1, 33.1, 33.1, 25.9, 25.8, 25.6, 25.5. ESI-MS *m/z* (%) 445 (100) $[M+H]^+$; Anal. Calcd for C26H31NS2 C, 74.06; H, 7.41; N, 3.32; Found: C, 74.09; H, 7.40; N, 3.31.

1,3-Bis((4-fluorophenyl)thio)-2-phenylindolizine (C10, 72 %)

Yellow oil. 64.1 mg. IR (KBr): 3141, 1551, 816, 747, 707 cm^{-1};^{1}H NMR (400 MHz, CDCl3) δ8.33 (d, *J* =7.2 Hz, 1 H), 7.70 (d, *J* =8.8 Hz, 1

H), 7.40 (d, *J* =1.6 Hz, 2 H), 7.33 (dd, *J* = 4.8, 2.8 Hz, 3 H), 7.05 (d, *J*

=7.6 Hz, 1 H), 6.97− 6.89 (m, 4 H), 6.89− 6.85 (m, 4 H), 6.76 (td, *J* =

6.8, 1.2 Hz,1 H). ^{13}C NMR (100 MHz, CDCl3) δ 162.5 (*J* =50.6 Hz), 160.1 (*J* =49.1 Hz), 141.5, 139.2, 134.8(*J* =2.9 Hz), 133.0, 131.4 (*J* =3.0 Hz), 130.5, 127.8, 127.7, 127.4 (*J* =8.1 Hz), 127.3 (*J* =7.9 Hz), 124.4, 122.4, 117.8, 116.5 (*J* =22.0 Hz), 115.9 (*J* =21.9 Hz), 112.9, 108.2, 98.3. ESI-MS *m/z* (%) 445 (100) $[M+H]^+$; Anal. Calcd for C26H17F2NS2 C, 70.09; H, 3.85; N, 3.14; Found: C, 70.08; H, 3.86; N, 3.15.

2-Phenyl-1,3-bis(p-tolylthio)indolizine (C11, 53 %)

Yellow oil. 46.3 mg. IR (KBr): 3034, 2904, 1601, 750, 725, 689 cm^{-1};^{1}H NMR (400 MHz, CDCl3) δ 8.33 (s, 1 H), 7.70 (d, *J* =8.8 Hz, 1 H), 7.45 (d, *J* =5.6 Hz, 2 H), 7.33 (d, *J* =6.8 Hz, 3 H), 7.07− 6.98 (m, 5 H), 6.93 (s, 2 H), 6.82 (d, *J* =8.0 Hz, 2 H), 6.74 (t, *J* =6.8 Hz, 1 H), 2.28 (s, 3 H), 2.27 (s, 3 H). ^{13}C NMR (100 MHz, CDCl3) δ 141.4, 139.2, 136.6, 135.4, 134.3, 133.3, 133.0, 130.5, 130.0, 129.5, 127.7, 127.5, 125.5, 125.4, 124.5, 122.0, 117.9, 112.6, 108.0, 97.8, 20.9, 20.8.ESI-MS *m/z* (%) 437 (100) $[M+H]^+$; Anal. Calcd for C28H23NS2 C, 76.85; H, 5.30; N, 3.20; Found: C, 76.82; H, 5.31; N, 3.21.

2,2′-((2-Phenylindolizine-1,3-diyl) bis(sulfanediyl)) dianiline (C12, 32 %)

Yellow oil. 28.1 mg. IR (KBr): 3354, 3041, 1551, 750, 707cm^{-1};^{1}H NMR (400 MHz, CDCl3) δ8.40 (d, *J* =7.2 Hz, 1 H), 7.75 (d, *J* =8.8 Hz, 1

H), 7.49 (d, *J* =6.8 Hz, 2 H), 7.40 (dd, *J* = 12.0, 7.2 Hz, 3 H), 6.96 (dt, *J* = 15.2, 7.2 Hz, 4 H), 6.87 (d, *J* =9.2 Hz, 1 H), 6.71(t, *J* =7.2 Hz, 1 H), 6.56 (dd, *J* = 14.8, 7.6 Hz, 4 H), 3.34 (s, 4 H). ^{13}C NMR (100 MHz, CDCl3) δ 145.7, 140.7, 138.9, 133.7, 131.4, 131.2, 130.8, 128.6, 128.1, 127.9, 127.7, 124.7, 121.9, 119.2, 119.1, 118.1, 116.1, 115.7, 112.7, 108.1, 98.9. ESI-MS *m/z* (%) 439 (100) $[M+H]^+$; Anal. Calcd for C26H21N3S2 C, 71.04; H, 4.82; N, 9.56; Found: C, 71.03; H, 4.81; N, 9.57.

2.5. Valuation of pharmacological activity

2.5.1. Cell viability experiments

Cells were harvested by trypsinization, and then seeded in a 96-well plate (10^4 cells per well) with medium and incubated overnight. Subsequently, the supernatant was removed, indicated compounds were added to the plate in numerous concentrations in medium supplemented with 10 % FBS. The control group was cultured in medium supplemented with 10 % FBS only. Twenty-four hours later, 5 μL of MTT (5 mg/mL) solution was added in 100 μL medium and incubated for 4 h according to MTT Kit. Absorbance was measured at 570 nm wavelength by a micro-plate reader (Thermo Labsystems, USA).

2.5.2. Hoechst 33342 staining

Cells were cultured in a 12-well plate (10^5 cells per well) for twenty- four hours, cells were treated with C8 (15, 30 μg/mL). 24 h later, 200 μL of staining solution of Hoechst 33342 was added to each well and incubated for 25 min at 37 °C incubator. Then the dye was discarded, cells in plates were washed three times with PBS. Pictures of cells were taken by the fluorescence microscope (Zeiss, Germany). The nucleus of apoptotic cells was densely stained or densely stained in pieces were observed.

2.5.3. Cell cycle analysis

Cells were cultured in a 6-well plate ($5*10^5$ cells per well) for twenty- four hours, then treated with C8 (15, 30 μg/mL) for 24 h (with or without 10 μM Pifithrin-α pretreatments for 1 h). According to guidance of the manufacturer's instructions, the supernatant and cells were collected, centrifuged 5 min at 1000 *g*. The supernatant was aspirated carefully, fixed in 70 % ethanol overnight at 4 °C, the cells were washed thrice with PBS and resuspended in 300 μL PBS. After that, 0.5 mL of propidium iodide dye was added to cell sample, resuspended slowly and fully, and kept at 37 °C for 30 min in the dark. The cell cycle distribution was determined using flow cytometry (CytoFlex, Beckman).

2.5.4. Annexin V/PI staining

Cells were cultured in a 6-well plate ($5*10^5$ per well) for 24 h, then incubated with C8 for 24 h (with or without 10 μM LY294002 pretreatments for 1 h). As previously described, cells stained with pre-incubation. The medium was aspirated into a tube, the adherent cells were washed with PBS, and

collected in the same tube, centrifuged at 1000 *g* for 5 min. The supernatant was discarded, precipitated cells mixed with apoptosis detection dye accordance with the instructions from Annexin V-FITC Apoptosis Detection Kit, incubated at room temperature for 20 min in the dark, then placed in an ice bath. Finally, the samples were determined for ratio of apoptotic cells by flow cytometry (CytoFlex, Beckman).

2.5.5. Detection of Reactive Oxygen Species (ROS) levels Cells were treated as mentioned above, harvested, and washed with PBS thrice. Cells were then incubated with 2′, 7-dichlorfluorescein-diacetate (DCFH-DA) in the dark for 30 min at 37 °C for ROS detection. The levels of intracellular ROS were determined according to the description of kit. The fluorescence intensity was detected via flow cytometry.

2.5.6. Estimation of Mitochondrial membrane potential (MMP)

After cells were exposed to C8 for 24 h as previously described, JC-1 staining was carried out according to the mitochondrial membrane potential assay kit with JC-1. Reactive oxygen species (ROS) deprivation group after the C8 (30 μg/mL) treatment, the supernatant was discarded, washed three times with PBS, and added ROS scavenger (N-acetyl-L-cysteine, NAC, 5 mM) for one-hour incubation. Cells were exposed to JC-1 for 30 min at 37 °C, and then fluorescent images were taken via the microscope.

2.5.7. Western blotting assay

Cells were treated as indicated, then washed with cold PBS and was lysed in lysis buffer (phosphatase and protease inhibitor mixture). Lysate samples were centrifuged at 12,000 *g* for 10 min at 4 °C, and the supernatant was collected. Determination of its protein concentration by bicinchoninic acid protein assay (BCA). Protein was separated by SDS- PAGE gels (Bio- Rad, USA) and transferred to PVDF membrane (Millipore, USA), protein in transferred membrane was blocked in 5% skimmed milk for 2 h, and then incubated with primary antibodies at 4 °C overnight. After being washed with TBST for 10 min thrice, the membranes were incubated with secondary antibodies for 1 h at room temperature. Washed as described above, then visualized the immunoblots via Gel 2000 image analyzer (Bio-Rad, USA). The protein expression level was analyzed using the ImageJ software.

2.6. Statistical analysis

All the experiments were performed independently three times. GraphPad Prism version 7 software was utilized to experimental data analysis. The results were presented as the mean ± SD. To assess the significant discrepancy of diverse groups, the one-way analysis of variance (ANOVA) and the Student's *t* test were carried out. Differences were considered significant at $^{**}P < 0.01$, $^{***}P < 0.001$, $^{****}P < 0.0001$.

3. Results

3.1. Chemistry

We reported previously that a direct C–H bond activation strategy was used to synthesize indolizine derivatives. The advantages of this method are simplicity, efficiency, and environmental protection. The results are outlined in Scheme (Fig. 1).

3.2. Capability of C8 to inhibit proliferation of A549 cells

To screen the antiproliferative activity of the series of the synthesized compounds on A549 cells, MTT assay was conducted, the screening concentration of the compounds refers to the highest concentration of the anticancer activity of drugs with similar structure to the compounds [13]. Among the selected twelve compounds, **C8** (**compound 8, dithiolation indolizine**) showed more significantly proliferative inhibition capacity than other compounds. We examined cytotoxic effect of C8 in gradient concentrations. The viability of cells of C8 group decreased suddenly after cells were incubated with C8 (15, 30 μg/mL), the selected concentrations of 15, 30 μg/mL were for further research (Fig. 2B). However, C8(15, 30 μg/mL) had little cytotoxicity in SH-SY5Y neuroblastoma cells, liver cancer HepG2 cells, and normal human bronchial epithelial BEAS-2B cells (Fig. 2C).

3.3. The nucleus morphological changes of A549 cells induced by C8

Hoechst binds to structurally damaged DNA fragments and emits stronger blue fluorescence [14]. Nucleus morphological changes were detected by Hoechst 33342 assay then imaged under a fluorescent microscope. The nuclei were densely stained by the dye, and even appeared to be fragmented, enhanced fluorescence intensity, as the concentration of the drug increased, which suggested the apoptosis of cells (Fig. 3).

3.4. C8 inhibits mitotic progression of A549 cells via p53 pathway The results of analysis of the cell cycle distribution illustrated that cell cycle was arrested by C8 in the G2-M phase (Fig. 4A and B). Moreover, sub G1 phase is considered as an important indicator of apoptosis [15], the proportion of sub G1 phase increased with drug concentration-dependence. The expression of PARP-1 protein declined (Fig. 4C). It was consistent with the obtained results (Fig. 3). Next, we found the increased expression of p53 proteins and the down-regulation of its

downstream gene CyclinB1 (Fig. 4C), which suggested p53 responded to DNA damages. Pifithrin-α(PF) can specifically inhibit p53-dependent gene transcription activation. Compared with the C8 group, the reduction of G2/M phase cells in the C8 + PF group, indicating that the inhibition of p53 by Pifithrin-α partially reversed the G2/M phase arrest of A549 cells by C8 (Fig. 5).Cyclin B1 is essential for G2/M phase transition [16], the down-regulation of which predominantly prevented the cells escaping G2/M process.

3.5. Apoptosis induced by C8

Experiments were conducted to quantify apoptosis effect of C8 on A549 cells, after incubated with C8 (15, 30 μg/mL) for 24 h. The results of flow cytometry showed that the proportion of cells of early apoptosis and the lately apoptosis increased (Fig. 6A), especially the increased ratio of the early apoptosis compared with the control group (Fig. 6B). One of the major pathways involved in cell survival is PI3K/Akt [17]. The data illustrated that the proportion of p-Akt/Akt decreased with the increase of C8 concentrations (Fig. 6C and D). Compared with the Akt inhibitor LY2942002 alone pretreatment group, there was no significant additional increase in the proportion of apoptosis in the combination group (C8 + LY group), it suggested that the apoptotic effect of the C8 on A549 cells were mediated via the PI3K/Akt pathway (Fig. 7). In addition, Caspase-3 is the indispensable terminal cleavage enzyme in the process of apoptosis [18]. PARP is one of the main cleavage targets of Caspase-3, the Cleaved-PARP can be regarded as a sign of apoptosis [19]. The Cleaved Caspase-3 and Cleaved PARP expressions were significantly increased, these data confirmed A549 cells apoptosis occurs (Fig. 6C and D).

3.6. Mitochondrial dysfunction and ROS accumulation in A549 cells induced by C8

JC-1 is a fluorescent probe for detecting mitochondrial membrane potential (MMP, ΔΨ). Compared to untreated group, a majority of JC-1 existed as monomer, emitted strong green fluorescence (Fig. 8D), the group of higher concentration of C8 showed a higher ratio of fluorescence intensity (green/red). Strong green fluorescence indicated that the MMP depolarization. Then we examined the expressions of apoptosis-associated proteins involved in mitochondrial pathway, pro-apoptotic proteins (Bax, Bim) of treatment groups increased, at the same time,

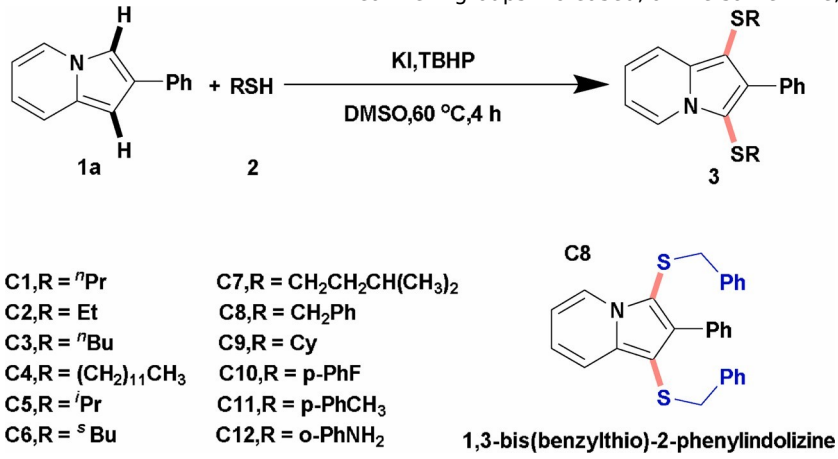

Fig. 1. Scheme for compound synthesis and structure diagram of Compound 8 (C8).

Fig. 2. Growth inhibition of selected compounds on the cell lines (A549, SH-SY5Y, HepG2, and BEAS-2B) using MTT assay. **(A)** 12 compounds were tested for the cell viability of A549 cells at a concentration of 50 μg/mL. C8 significantly inhibit the proliferation of A549 cells. **(B)** Cell viability decreased in drug concentration- dependence manner after cells incubated with C8. (**C**) The sensitivity of C8 to different cell lines (SH-SY5Y, HepG2, and BEAS-2B cells) were tested. The data were expressed as mean ± S.D. (n = 3).

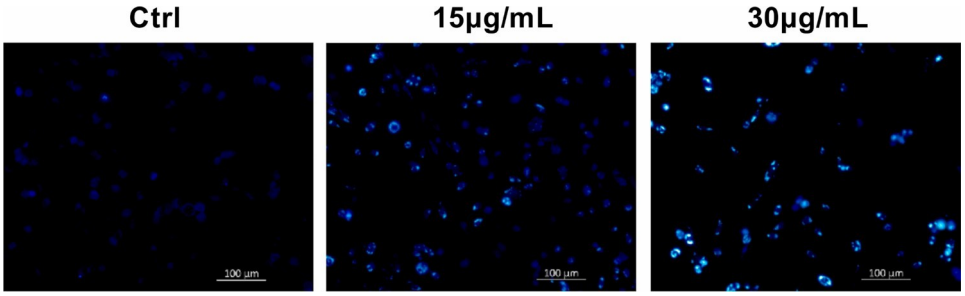

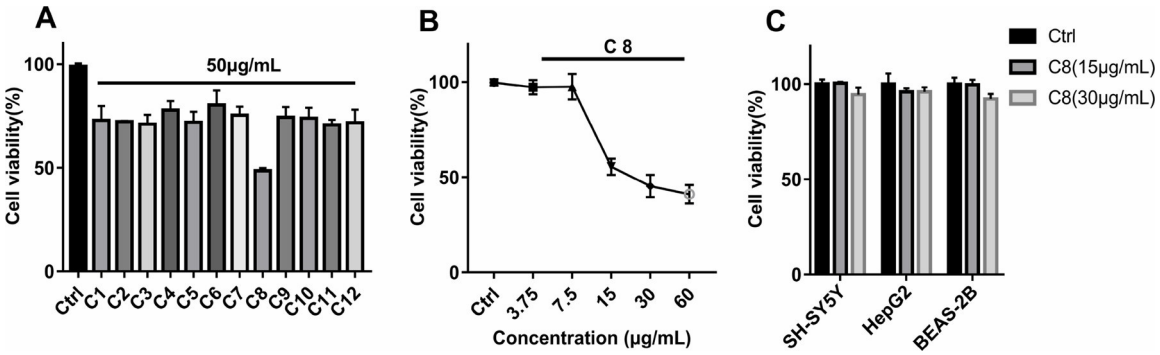

Fig. 3. Changes in nuclear morphology. Cells stained with Hoechst 33342 were pictured by fluorescence microscope, after incubated with C8 at the concentrations of (15 and 30 μg/mL), which showed the apoptosis of cells (scale bar = 100 μm).

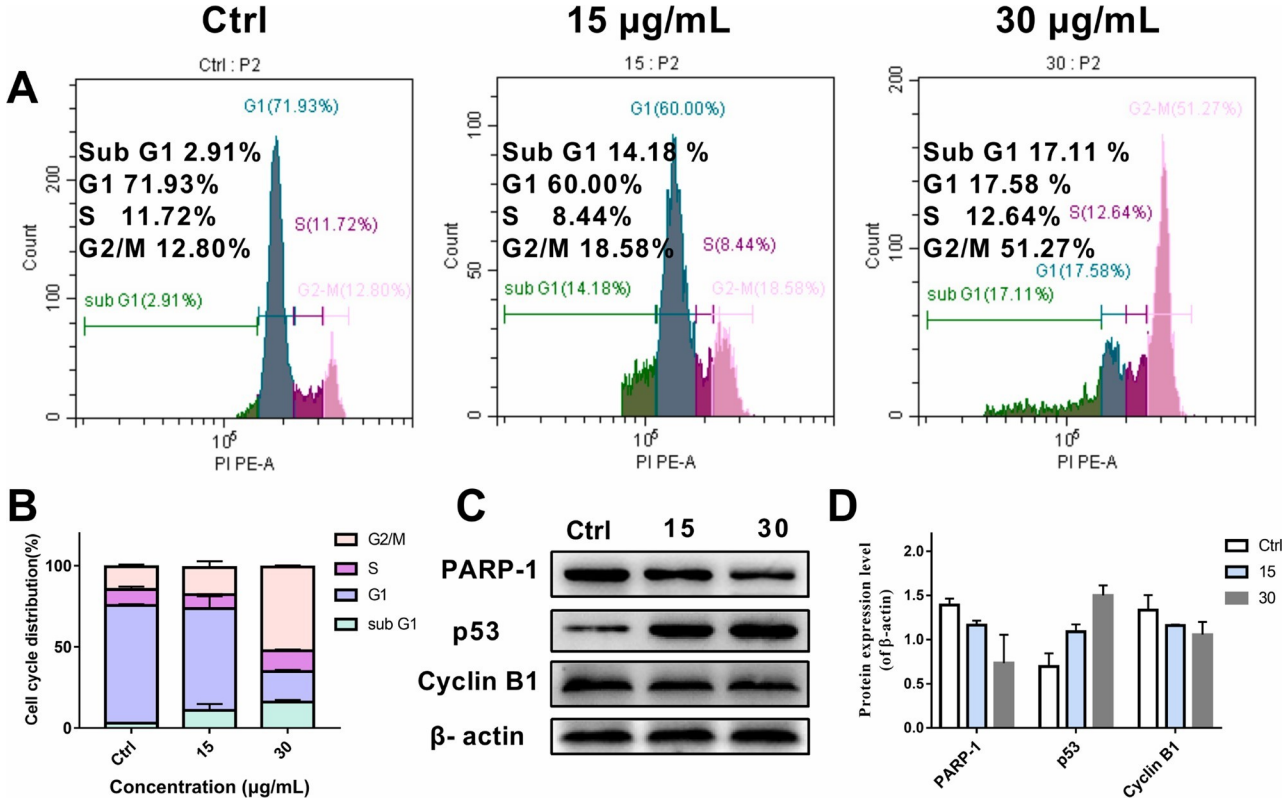

Fig. 4. Induction of cell cycle arrested at G2/M phase after incubated with C8. **(A)** Results were presented by CytoExpert software. **(B)** The proportion of cells in the G2/M phase increased with concentration-dependent. **(C)** Cell cycle-associated proteins were detected by Western blotting. **(D)** G2/M phase arrest related protein levels were analyzed. The data were expressed as mean ± S.D. (n = 3).

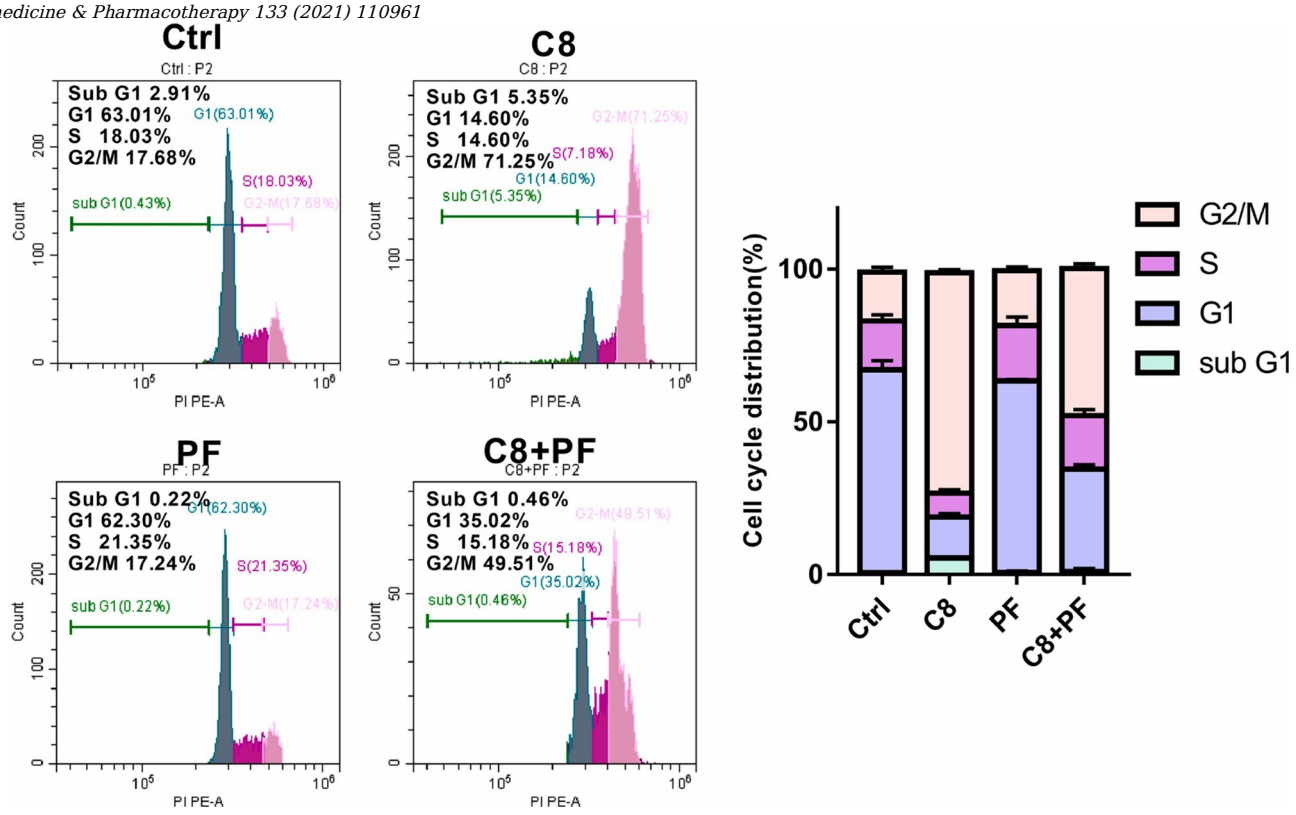

Fig. 5. Inhibition of p53 blocked C8(30 μg/mL)-induced G2/M phase arrest in A549 cells. The quantification of cells in different phases is presented as a percentage; C8 + Pifithrin-α(C8 + PF). The data were expressed as mean ± S.D. (n = 3).

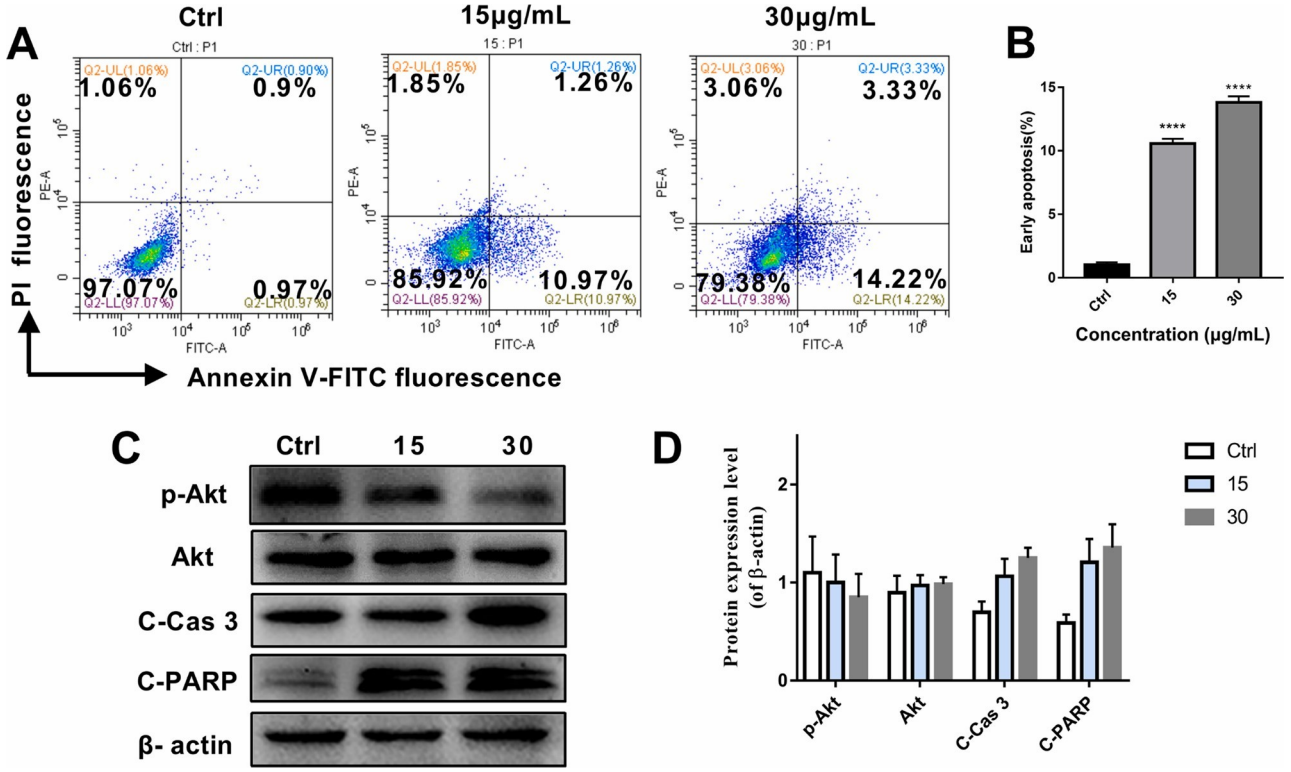

Fig. 6. The apoptosis of A549 cells induced by C8. **(A)** The apoptosis ratio of A549 cells was determined by flow cytometry. The ratios of early apoptosis (lower right quadrant) and the late apoptosis (upper right quadrant) were presented. **(B)** Increase of the early apoptosis ratio of A549 cells treated with C8 was shown. **(C)** Western blotting analyzed the expression of p-Akt, Akt, Cleaved-Caspase 3 (C-Cas 3,17 kDa), Cleaved-PARP (C-PARP,89 kDa) proteins after incubated with C8. **(D)** Quantify relative protein expressions were proceeded with grayscale analysis. The data were expressed as mean ± S.D. (n = 3). ****$P < 0.0001$ compared to the control group.

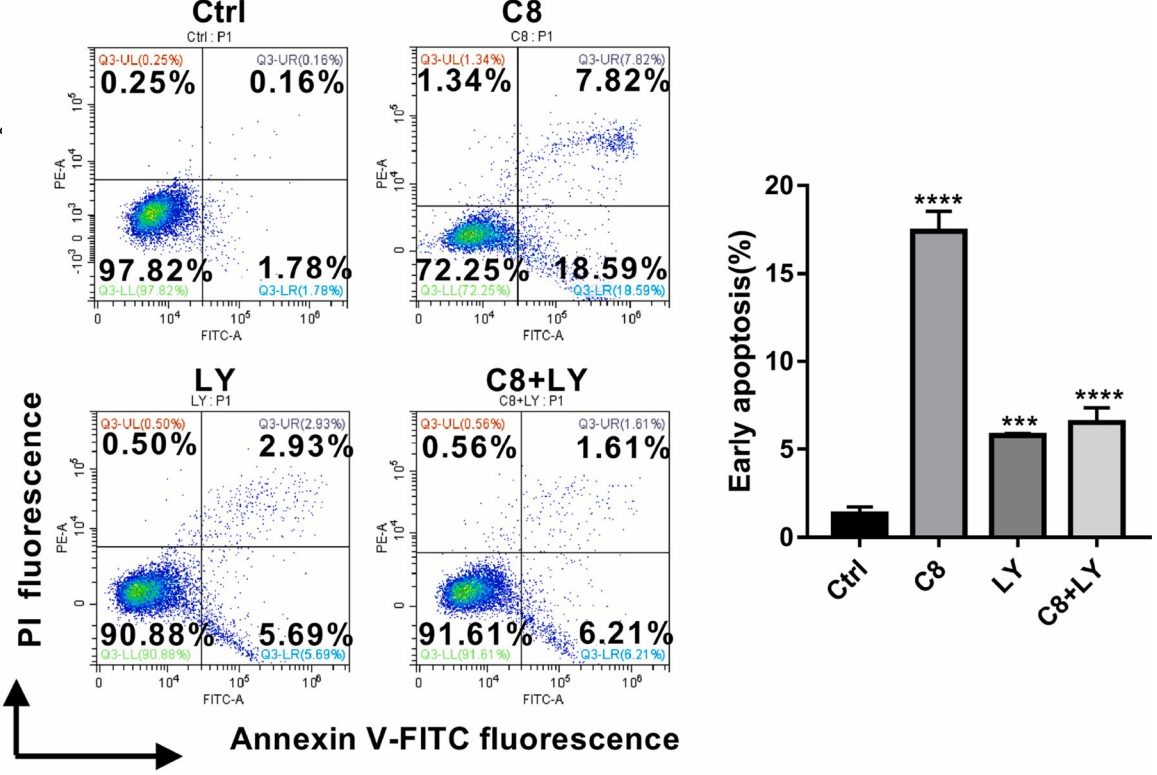

Fig. 7. Inhibition of Akt phosphorylation blocked C8(30 μg/mL)-induced apoptosis in A549 cells. C8 + LY294002 (C8 + LY). The data were expressed as mean ± S.D.
(n = 3). ***$P < 0.001$, ****$P < 0.0001$ compared to the control group.

expressions of apoptotic-resistance proteins (Bcl-2) decreased, and more Cytochrome C released to the cytoplasm. Additionally, the elevation of Caspase-12 expression indicated that C8 induced apoptosis via triggering endoplasmic reticulum stress (ERS) [20] (Fig. 8E).

Changes in intracellular ROS levels were specifically recognized by DCFH-DA fluorescent probes by flow cytometry. The results manifested a significant discrepancy between the treated groups and the control group on green fluorescence (Fig. 8A and B), which directly implicated with the ROS levels. The ROS levels of the C8 group (1530 μg/mL) increased. In order to investigate whether the accumulation of ROS levels of treatment groups impacted the depolarization of MMP, C8 (30 μg/mL) +NAC group (NAC: ROS deprivation agent) was used as another group to detect the loss of MMP escaped (Fig. 8D).

4. Discussion

Disordered reproduction and apoptotic resistance are the prominent characteristics of cancer cells, inhibiting cell proliferation and inducing apoptosis in the lesion are promising strategies for cancer therapy [21]. The results of our studies showed that cell growth of A549 cells was inhibited compared to the untreated group via MTT assay (Fig. 2B). Numerous studies suggested that disruption of cell cycle progression is considered an effective strategy to inhibit proliferation in cancer cells [22,23]. The overexpression of CyclinB1 protein accelerated G2/M phase transition and even resulted in abnormal proliferation in cancer cells [24]. C8 induced A549 cells to stagnate at G2/M phase, which was mediated by the collapse of CyclinB1 expression (Fig. 4A). Based on the results, we wondered how the blocking was mediated by Cyclin B1. We found that the cell cycle arrest was mediated in a p53-dependent manner. Tumor suppressor protein, p53 exerts critical function in the cells which is responded to DNA damages and other genomic aberrations [25,26]. Activation of p53 leads to cell cycle arrest, DNA repair, and apoptosis [15,27]. Obviously visible morphological changes were observed with C8 treatment, such as cell contraction, chromatin condensation and DNA fragmentation in varying degrees (Fig. 3), which consisted with the reduction of PARP-1 protein expression levels detected by Western blotting (Fig. 4c). PARP-1 is an important factor for cell survival and chromosomal stability [28]. Hence, we thought that the G2/M phase arrest by C8 on A549 cells was achieved by inhibiting DNA repair enzymes or disrupt the DNA repair system, then activating p53 and further repressing the downstream gene Cyclin B1 (Fig. 4C).

The results of flow cytometry (Fig. 6A and B) showed that the apoptosis ratio of A549 cells increased from 1.037 ± 0.1795 % (untreated group), 10.57 ± 0.3691 % (C8, 15 μg/mL) to 13.81 ± 0.4747 % (C8, 30 μg/mL), sequentially. Expression of Cleaved- Caspase-3, Cleaved-PARP indicated the apoptosis of cells [29]. Further analysis (Akt inhibitor LY294002 pretreatment) showed PI3K-Akt pathway involved in the apoptosis of A549 cells. Western blotting results indicated that after treatment, the expression of phosphorylated Akt (Fig. 6C and D) decreased (Fig. 8E and F). The pro-apoptotic protein Bim resided in the cytoplasm, and combined to Bax, would translocate into mitochondria after receiving death signals, antagonized the anti-apoptotic effect of Bcl-2, and then promoted the release of cytochrome C from mitochondria [30] (Fig. 8E and F).

Mitochondria are central processor in the processes of energy metabolism, cell signal transduction and apoptosis regulation [31,32]. Bcl-2 family proteins regulate mitochondrial apoptotic pathways [33]. When apoptosis of cells was induced by external factors, the permeable mitochondria outer membrane is regarded as an irreversible landmark, which is the execution of apoptotic procedures as the activation of mitochondrial

pathway [34,35]. Many studies have displayed that triggering apoptosis with mitochondrial channel/pore regulators become an available method for therapy of resistant cancer [29,36]. The above results mentioned that loss of MMP enabled mitochondrial outer membrane permeabilization (Fig. 8D).

Mitochondria of tumor cells are different from those of normal cells in terms of structure and function [37]. Mitochondria is the main organelles that produce ROS [38]. The medium-level ROS in tumor cells

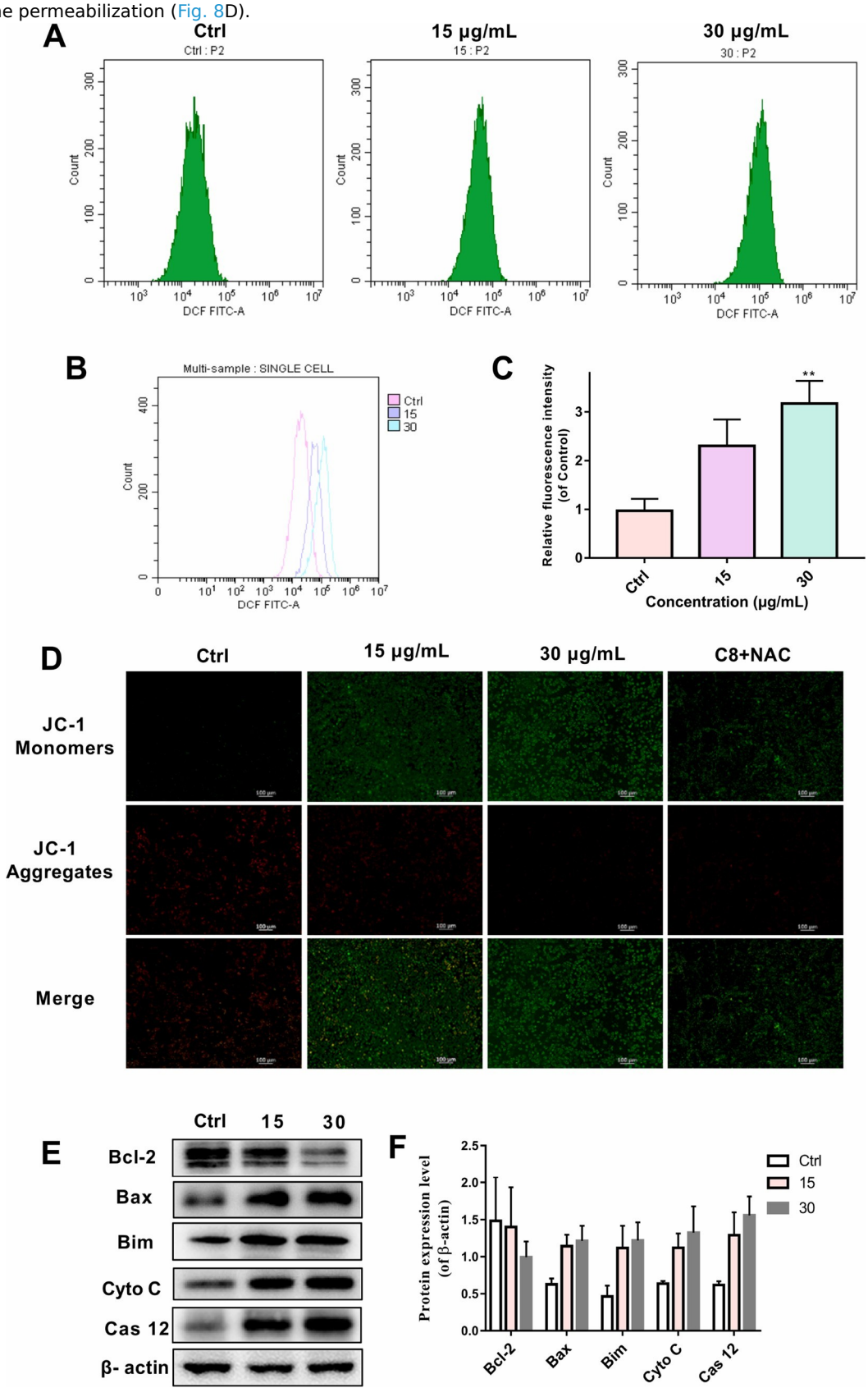

Fig. 8. Apoptosis of A549 cells treated with C8 by intrinsic mitochondrial pathway. **(A)** Intracellular ROS was detected by flow cytometry. **(B)** The fluorescence intensity was positively correlated with the levels of cellular ROS in three groups. **(C)** Accumulation of intracellular ROS levels after administration of C8 were presented with histogram results. **(D)** The cells were stained with JC-1 dye to estimate the ratio of green /red fluorescence (scale bar = 100 μm). **(E)** The expressions of proteins about mitochondrial-endoplasmic reticulum stress pathway-related were analyzed. **(F)** Relative levels of protein expression were detected in A549 cells. The data were expressed as mean ± S.D. (n = 3). ** $P < 0.01$ compared to the control group (For interpretation of the references to colour in this figure legend, the reader is referred to the web version of this article.).

maintains metabolism. However, excessive ROS produced by external stimuli is not conducive to the survival of cells, causing the accumulation of ROS and membrane potential abnormalities [39], lots of studies have confirmed that inhibition of the PI3K-Akt signal in cancer cells impeded the biofilm redox system [40]. Its downstream protein Bax depolarizes potassium inflow, resulting in loss of mitochondrial membrane potential (Δψm) and increased release of ROS [41]. It was clear that drug-stimulated ROS was involved in mitochondrial damage. Although the mechanism of ROS production was complicated, the obtained information was that the loss of mitochondrial membrane potential was improved when ROS deprivation agents was used. The mitochondrial dysfunction in cancer cells may also lead to the production of ROS, which could promote the dissociation and release of cytochrome C.

Caspase12 is the unique member of Caspase family that locates on endoplasmic reticulum (ER) membrane and is a key protein that mediates ER stress apoptosis [42]. Studies have shown that mice knocked out of Caspase12 are resistant to ER-induced apoptosis, Caspase12 is a specific molecule in ERS-mediated apoptosis. Numerous researches supported that the endoplasmic reticulum stress pathway interconnected with mitochondrial apoptotic pathways [43–45]. This may be related to the involvement of Caspase12 in mediating the Bcl-2 family [46].

From the above facts, we supported that the C8 induced apoptosis in A549 cells by activating endoplasmic reticulum stress and the mitochondrial pathway. Both are intrinsic apoptotic pathways.

The occurrence and development of non-small cell lung cancer (NSCLC) is a complex, multi- gene involved, multi- factorial process [26]. Various therapeutic schedules were taken into consideration to clinical treatment, but the cure rate remain unsatisfactory. Therefore, it is necessary to develop natural products or chemical candidates for the therapy of NSCLC. We demonstrated that the utilization of newly synthesized indolizine derivative had the repression of proliferation by cycle arrest and apoptosis in intrinsic pathways, we will modify the molecular structure of them and try to use appropriate dosage form for animal models of NSCLC in further studies.

5. Conclusion

Our research showed that an indolizine derivative, was synthesized by a novel method, exerted its cytotoxic effects on non-small lung cells (A549 cells). Therefore, we propose the compound as a promising candidate for anti-non-small cell lung cancer, which is worthy of further research and development.

CRediT authorship contribution statement

Guanting Li: Investigation, Data curation, Formal analysis, Software, Writing - original draft. **Xianwei Wu:** Investigation, Data curation. **Peng Sun:** Methodology. **Zhiyang Zhang:** Investigation. **Enxian Shao:** Investigation. **Jianping Mao:** Investigation. **Hua Cao:** Project administration, Resources. **Hongliang Huang:** Conceptualization, Funding acquisition, Resources, Supervision, Project administration, Validation, Visualization, Writing - review & editing.

Declaration of Competing Interest

The authors report no declarations of interest.

Acknowledgements

This work was supported by the Fund of Guangdong Provincial Department of Science and Technology (2013B021800083). This work was also supported by Key Laboratory of New Drug Discovery and Evaluation of ordinary universities of Guangdong province (No. 2017KSYS002), the Innovation Team Projects in Universities of Guangdong Province (No. 2018KCXTD016). It is also partly funded by a project “Innovation and university promotion project of Guangdong Pharmaceutical University through No. 2017KCXTD020”.

References

[1] R. Karuppasamy, S. Veerappapillai, S. Maiti, W.H. Shin, D. Kihara, Current progress and future perspectives of polypharmacology : from the view of non-small cell lung cancer, Semin. Cancer Biol. (2019).
[2] Z. Wu, Z. Yang, Y. Dai, Q. Zhu, L.A. Chen, Update on liquid biopsy in clinical management of non-small cell lung cancer, Onco. Ther. 12 (2019) 5097–5109.
[3] D.H. Shin, D.G. Leem, J.S. Shin, J.I. Kim, K.T. Kim, S.Y. Choi, M.H. Lee, J.H. Choi, K.T. Lee, Compound K induced apoptosis via endoplasmic reticulum Ca(2+) release through ryanodine receptor in human lung cancer cells, J. Ginseng Res. 42 (2) (2018) 165–174.
[4] M. Imran, A. Rauf, Z.A. Shah, F. Saeed, A. Imran, M.U. Arshad, B. Ahmad, S. Bawazeer, M. Atif, D.G. Peters, M.S. Mubarak, Chemo-preventive and therapeutic effect of the dietary flavonoid kaempferol: a comprehensive review, Phytother. Res. 33 (2) (2019) 263–275.
[5] Y.M. Shen, P.C. Lv, W. Chen, P.G. Liu, M.Z. Zhang, H.L. Zhu, Synthesis and antiproliferative activity of indolizine derivatives incorporating a cyclopropylcarbonyl group against Hep-G2 cancer cell line, Eur. J. Med. Chem. 45 (7) (2010) 3184–3190.
[6] Y. Hu, C. Zhang, X. Zhao, Y. Wang, D. Feng, M. Zhang, H. Xie, (+/-)-Homocrepidine A, a pair of anti-inflammatory enantiomeric octahydroindolizine alkaloid dimers from dendrobium crepidatum, J. Nat. Prod. 79 (1) (2016) 252–256.
[7] K.M. Attalah, A.N. Abdalla, A. Aslam, M. Ahmed, M.A.S. Abourehab, N.A. ElSawy, A.M. Gouda, Ethyl benzoate bearing pyrrolizine/indolizine moieties: design, synthesis and biological evaluation of anti-inflammatory and cytotoxic activities, Bioorg. Chem. (2019), 103371.
[8] K.N. Venugopala, C. Tratrat, M. Pillay, F.M. Mahomoodally, S. Bhandary, D. Chopra, M.A. Morsy, M. Haroun, B.E. Aldhubiab, M. Attimarad, A.B. Nair, N. Sreeharsha, R. Venugopala, S. Chandrashekharappa, O.I. Alwassil, B. Odhav, Anti-tubercular activity of substituted 7-methyl and 7-formylindolizines and in silico study for prospective molecular target identification, Antibiotics 8 (4) (2019).
[9] L. Han, C. Gao, Y. Jiang, P. Guan, J. Liu, L. Li, L. Xu, X. Huang, Jiangrines A-F and jiangolide from an actinobacterium, Jiangella gansuensis, J. Nat. Prod. 77 (12)

(2014) 2605–2610.
[10] V.B. Tatipamula, M.K. Kolli, S.B. Lagu, K.R. Paidi, R.R. P, R.P. Yejella, Novel indolizine derivatives lowers blood glucose levels in streptozotocin-induced diabetic rats: a histopathological approach, Pharmacol. Rep. 71 (2) (2019) 233–242.
[11] Y. Xue, J. Tang, X. Ma, Q. Li, B. Xie, Y. Hao, H. Jin, K. Wang, G. Zhang, L. Zhang, L. Zhang, Synthesis and biological activities of indolizine derivatives as alpha-7 nAChR agonists, Eur. J. Med. Chem. 115 (2016) 94–108.
[12] B. Li, Z. Chen, H. Cao, H. Zhao, Transition-metal-Free regioselective cross-coupling: controlled synthesis of mono- or dithiolation indolizines, Org. Lett. 20 (11) (2018) 3291–3295.
[13] Y. Liu, E. Shao, Z. Zhang, D. Yang, G. Li, H. Cao, H. Huang, A novel indolizine derivative induces apoptosis through the mitochondria p53 pathway in HepG2 cells, Front. Pharmacol. 10 (2019) 762.
[14] J. Wu, P. Apontes, L. Song, P. Liang, L. Yang, F. Li, Molecular mechanism of upregulation of survivin transcription by the AT-rich DNA-binding ligand, Hoechst33342: evidence for survivin involvement in drug resistance, Nucleic Acids Res. 35 (7) (2007) 2390–2402.
[15] D.K.F. Silva, S.S. Duarte, T.M.H. Lisboa, R.C. Ferreira, A.L.O. Lopes, D.C. M. Carvalho, S. Rodrigues-Mascarenhas, P.M. da Silva, M. Segundo, R.O. Moura, K. C.P. Medeiros, M.V. Sobral, Antitumor effect of a novel spiro-acridine compound is associated with up-regulation of Th1-type responses and antiangiogenic action, Molecules 25 (1) (2019).
[16] E.K. Choi, J.A. Lim, J.K. Kim, M.S. Jang, S.E. Kim, H.J. Baek, E.J. Park, T.H. Kim, C. X. Deng, R.H. Wang, S.S. Kim, Cyclin B1 stability is increased by interaction with BRCA1, and its overexpression suppresses the progression of BRCA1-associated mammary tumors, Exp. Mol. Med. 50 (10) (2018) 1–16.
[17] G. Hoxhaj, B.D. Manning, The PI3K–AKT network at the interface of oncogenic signalling and cancer metabolism, Nat. Rev. Cancer (2019).
[18] L. Lossi, C. Castagna, A. Merighi, Caspase-3 mediated cell death in the normal development of the mammalian cerebellum, Int. J. Mol. Sci. 19 (12) (2018).
[19] D.S. Kim, S. Challa, A. Jones, W.L. Kraus, PARPs and ADP-ribosylation in RNA biology: from RNA expression and processing to protein translation and proteostasis, Genes Dev. 34 (5–6) (2020) 302–320.
[20] J. Song, Q. Zhang, S. Wang, F. Yang, Z. Chen, Q. Dong, Q. Ji, X. Yuan, D. Ren, Cleavage of caspase-12 at Asp94, mediated by endoplasmic reticulum stress (ERS), contributes to stretch-induced apoptosis of myoblasts, J. Cell. Physiol. 233 (12) (2018) 9473–9487.
[21] P. Lu, Q. Ding, X. Li, X. Ji, L. Li, Y. Fan, Y. Xia, D. Tian, M. Liu, SWELL1 promotes cell growth and metastasis of hepatocellular carcinoma in vitro and in vivo, EBioMedicine 48 (2019) 100–116.
[22] N. Mendez-Barbero, C. Gutierrez-Munoz, J. Madrigal-Matute, P. Minguez, J. Egido, J.B. Michel, J.L. Martin-Ventura, V. Esteban, L.M. Blanco-Colio, A major role of TWEAK/Fn14 axis as a therapeutic target for post-angioplasty restenosis, EBioMedicine 46 (2019) 274–289.
[23] D. Yang, Q. Zhang, Y. Ma, Z. Che, W. Zhang, M. Wu, L. Wu, F. Liu, Y. Chu, W. Xu, M. McGrath, C. Song, J. Liu, Augmenting the therapeutic efficacy of adenosine against pancreatic cancer by switching the Akt/p21-dependent senescence to apoptosis, EBioMedicine 47 (2019) 114–127.
[24] J. Chen, L. Li, J. Su, B. Li, X. Zhang, T. Chen, Proteomic analysis of G2/M arrest triggered by natural borneol/curcumin in HepG2 cells, the importance of the reactive oxygen species-p53 pathway, J. Agric. Food Chem. 63 (28) (2015) 6440–6449.
[25] H. Du, Y. Huang, X. Hou, X. Quan, J. Jiang, X. Wei, Y. Liu, H. Li, P. Wang, M. Zhan, X. Ai, L. Lu, S. Yuan, L. Sun, Two novel camptothecin derivatives inhibit colorectal cancer proliferation via induction of cell cycle arrest and apoptosis in vitro and in vivo, Eur. J. Pharm. Sci. 123 (2018) 546–559.
[26] H. Loffler, J. Lukas, J. Bartek, A. Kramer, Structure meets function–centrosomes, genome maintenance and the DNA damage response, Exp. Cell Res. 312 (14) (2006) 2633–2640.
[27] J.Y. Tsai, S.H. Tsai, C.C. Wu, The chemopreventive isothiocyanate sulforaphane reduces anoikis resistance and anchorage-independent growth in non-small cell human lung cancer cells, Toxicol. Appl. Pharmacol. 362 (2019) 116–124.
[28] M. Akpolat, Z.S. Oz, K. Gulle, A.C. Hamamcioglu, B.H. Bakkal, M. Kececi, X irradiation induced colonic mucosal injury and the detection of apoptosis through PARP-1/p53 regulatory pathway, Biomed. Pharmacother. 127 (2020), 110134.
[29] U. Vijapurkar, W. Wang, R. Herbst, Potentiation of kinesin spindle protein inhibitor-induced cell death by modulation of mitochondrial and death receptor apoptotic pathways, Cancer Res. 67 (1) (2007) 237–245.
[30] I. Vivanco, C.L. Sawyers, The phosphatidylinositol 3-Kinase AKT pathway in human cancer, Nat. Rev. Cancer 2 (7) (2002) 489–501.
[31] T. Wai, T. Langer, Mitochondrial dynamics and metabolic regulation, Trends Endocrinol. Metab. 27 (2) (2016) 105–117.
[32] S. Pickles, P. Vigie, R.J. Youle, Mitophagy and quality control mechanisms in mitochondrial maintenance, Curr. Biol. 28 (4) (2018) R170–R185.
[33] F.J. Bock, S.W.G. Tait, Mitochondria as multifaceted regulators of cell death, Nat. Rev. Mol. Cell Biol. (2019).
[34] J. Song, C. Lin, X. Yang, Y. Xie, P. Hu, H. Li, W. Zhu, H. Hu, Mitochondrial targeting nanodrugs self-assembled from 9-O-octadecyl substituted berberine derivative for cancer treatment by inducing mitochondrial apoptosis pathways, J. Control. Release 294 (2019) 27–42.
[35] D. Hanahan, R.A. Weinberg, Hallmarks of cancer: the next generation, Cell 144 (5) (2011) 646–674.
[36] R. Peruzzo, I. Szabo, Contribution of mitochondrial ion channels to chemo- resistance in cancer cells, Cancers 11 (6) (2019).
[37] T. Haider, R. Tiwari, S.P. Vyas, V. Soni, Molecular determinants as therapeutic targets in cancer chemotherapy: an update, Pharmacol. Ther. 200 (2019) 85–109. [38] X. Zhai, S. Yuan, X. Yang, P. Zou, L. Li, G. Li, Y. Shao, A.M. Abd El-Aty, A. Hacimuftuoglu, J. Wang, Chitosan oligosaccharides induce apoptosis in human renal carcinoma via reactive-oxygen-species-dependent endoplasmic reticulum stress, J. Agric. Food Chem. 67 (6) (2019) 1691–1701.
[39] Q. Cui, J.Q. Wang, Y.G. Assaraf, L. Ren, P. Gupta, L. Wei, C.R. Ashby Jr., D.H. Yang, Z.S. Chen, Modulating ROS to overcome multidrug resistance in cancer, Drug Resist. Updat. 41 (2018) 1–25.
[40] X. Xu, Y. Zhang, D. Qu, T. Jiang, S. Li, Osthole induces G2/M arrest and apoptosis in lung cancer A549 cells by modulating PI3K/Akt pathway, J. Exp. Clin. Cancer Res. 30 (2011) 33.
[41] Y. Yang, S. Karakhanova, W. Hartwig, J.G. D'Haese, P.P. Philippov, J. Werner, A. V. Bazhin, Mitochondria and mitochondrial ROS in cancer: novel targets for anticancer therapy, J. Cell. Physiol. 231 (12) (2016) 2570–2581.
[42] S.V.S. Rana, Endoplasmic reticulum stress induced by toxic elements-a review of recent developments, Biol. Trace Elem. Res. (2019).
[43] R. Ushioda, K. Nagata, Redox-mediated regulatory mechanisms of endoplasmic reticulum homeostasis, Cold Spring Harb. Perspect. Biol. 11 (5) (2019).
[44] A.F. Abdel-Wahab, W. Mahmoud, R.M. Al-Harizy, Targeting glucose metabolism to suppress cancer progression: prospective of anti-glycolytic cancer therapy, Pharmacol. Res. 150 (2019), 104511.
[45] C. Guo, R. Ma, X. Liu, Y. Xia, P. Niu, J. Ma, X. Zhou, Y. Li, Z. Sun, Silica nanoparticles induced endothelial apoptosis via endoplasmic reticulum stress- mitochondrial apoptotic signaling pathway, Chemosphere 210 (2018) 183–192.
[46] R. Li, Y. Yang, P. Hong, Z. Zhang, L. Li, J. Hui, X. Zheng, Beta-carotene attenuates weaning-induced apoptosis via inhibition of PERK-CHOP and IRE1-JNK/p38 MAPK signalling pathways in piglet jejunum, J. Anim. Physiol. Anim. Nutr. (Berl.) (2019).